

## Effect of Short Term Aging on Microstructure Evolution, Pitting and Intergranular Corrosion Behaviour of UNS31254

Yipeng Liu<sup>1</sup>, Ning Zhong<sup>2</sup>, YangTing Sun<sup>1</sup>, Yiming Jiang<sup>1,\*</sup>

<sup>1</sup> Department of Materials Science of Fudan University, Shanghai, PR China

<sup>2</sup> Institute of Marine Materials Science and Engineering of Shanghai Maritime University, Shanghai, PR China

\*E-mail: [ymjiang@fudan.edu.cn](mailto:ymjiang@fudan.edu.cn)

Received: 24 February 2016 / Accepted: 19 March 2016 / Published: 1 April 2016

---

Here the intergranular and pitting corrosion resistance of super austenitic stainless steel Type UNS31254 was investigated, whose performance declined obviously after aging at 900 °C for short terms. Test methods including the nitric acid immersion test and the potentiostatic pulse technique (PPT) were applied respectively, and the results showed that the samples were highly sensitive to those two types of localized corrosion after aging within 180 minutes. Then the segregation between the interior and boundaries of grains eased while the general corrosion became dominated. The transmission electron microscope (TEM) further revealed molybdenum-rich Laves-related phases formed along the boundaries for only 10 minutes and they were the main culprit for the degradation. Finally, to offer guidance for the process of UNS31254, the welding joints were also checked and the evaluation method of pitting corrosion was discussed.

---

**Keywords:** Super Austenitic Stainless steel; Pitting corrosion; Precipitation; Potentiostatic Pulse Technique

### 1. INTRODUCTION

Compared with ordinary austenitic stainless such as 300-series, super austenitic stainless steel (SASS) Type UNS31254 has drawn much more attention because of providing an excellent combination of mechanical properties and corrosion resistance within a wide temperature range [1]. UNS31254 exhibits outstanding impact toughness and high strength, and also offers high resistance to localized corrosion due to its high level of nickel and molybdenum contents. Therefore, it has been widely used as structural materials in several marine applications such as piping and heat exchangers, which handle seawater containing Cl<sup>-</sup> [2-7]. It has also been extensively used in other aggressive media

for making some critical components like tubulars in petroleum industry, chemical and power industry [8-12]. Besides, since UNS31254 is a technically adequate substitute for nickel-based alloys in several conditions [13], it is more economical environmentally friendly. However, detrimental secondary phases can be rapidly formed at evaluated temperatures for high alloy UNS31254, which consequently deteriorate both mechanical properties and corrosion resistance. So attention must be paid to avoid forming damaging amounts of these phases during operations such as annealing, welding or explosion cladding.

In previous studies, some basic parameters of Type UNS31254 localized corrosion resistance in chloride contained solutions have gained, like critical pitting and crevice temperature of the matrix [4, 11, 14-17], simulating the seawater environment of its application. Recently, researches have been done to understand its precipitation behaviour and mechanical performance after long-term aging. The stable  $\sigma$  phase is deemed as the dominant intermetallic phase under the treatment with temperature higher than 850 °C [18], and its existence contributes to the decline of toughness [19, 20]. Other typical ones such as  $\chi$  and Laves-type phases have been found as well, and the conclusions demonstrate that these metastable phases form at lower temperature and could finally transform into  $\sigma$  phase [18, 21, 22]. All these phases result in an increase of both yield stress and ultimate tensile stress. Nevertheless, most of the existing work has analysed its pitting and intergranular corrosion behaviour or microstructure evolution separately and little research has been devoted to associate them together, especially the results after short term aging.

Hence, the objective of present work attempts to investigate the negative effects that the precipitations bring to the intergranular and pitting corrosion resistance of UNS31254 at 900°C, the most sensitive temperature of its time-temperature-precipitation curves. Besides the traditional test methods, the potentiostatic pulse technique (PPT) is also introduced in the present work to detect the weak point of passive film and the precipitation sites. This technique has been widely used in the investigation of organic coating failure [23, 24], and here aims to induce the formation of stable pits at the certain sites, where secondary phases form and the passive film becomes discontinuous [25, 26]. Based on the identification of these phases, the relation between precipitation behaviour and corrosion resistance is clear, further providing guidance for the application or production of UNS31254.

## 2. EXPERIMENTAL PROCEDURES

### 2.1. Specimens and heat treatment

The investigated material was a commercial SASS plate (approximately 5mm thickness) of type UNS31254, whose composition was shown in Table 1. The plate was cut into 20mm × 30mm specimens for the immersion test and 12mm × 12 mm for critical pitting temperature (CPT) tests. Then the as received specimens were submitted to heat treatment at 900 °C for different timings (10, 30, 60, 90, 180 and 360 minutes). The Gleeble3800 Thermal Simulator was also applied to simulate the welding heat curve shown in Fig.1. With different cooling rate and heat input, which are also the frequent-used parameters for welding process, the samples experienced diverse thermal cycling and

passed through the sensitive temperature range briefly. Next, the specimens for electrochemical tests were embedded in epoxy resin and grounded mechanically from 180 to 2000 grit. They were subsequently polished with diamond pastes of 2.5 $\mu$ m and 1.5 $\mu$ m granulation, then remained the exposure area of 1cm<sup>2</sup> after degreased with ethanol and blow-dried.

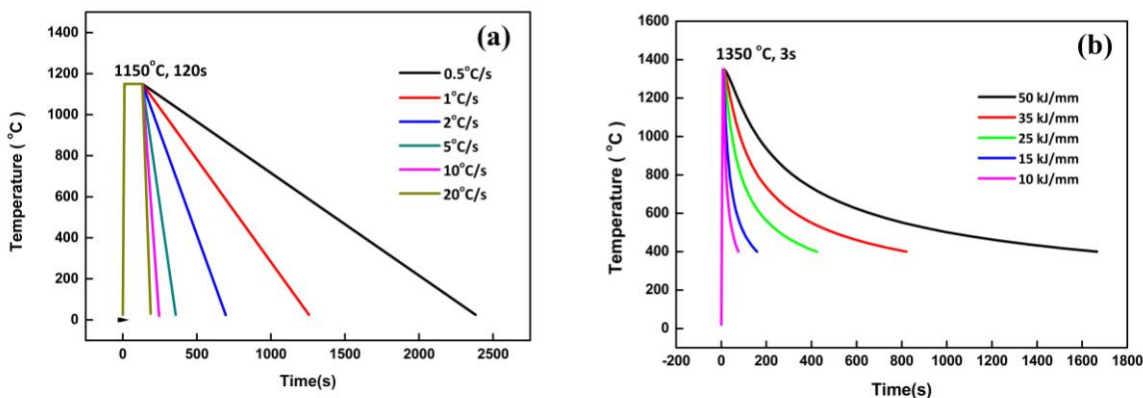


Figure 1. The welding heat curves for simulation.

Table 1 The chemical compositions of UNS31254 (wt %).

C	Cr	Ni	Mo	N	Cu	S	P	Si	Mn	Fe
<0.020	19.5	17.5	6.0	0.18	0.5	<0.01	<0.03	<0.8	<1.0	Bal.

2.2. Localized corrosion tests

2.2.1 Intergranular corrosion test

The boiling 65wt% nitric acid solution was selected for testing susceptibility of intergranular corrosion, which offered a potential near the transpassivation region of Tafel polarization curve. This test could detect the low-chromium zone and dissolve molybdenum-rich phases combining with the weight loss. Referring to the standard ASTM A262-C [27], the test was divided into two periods. Each of them lasted 48 hours and the solution was renewed every period keeping the same samples on test.

2.2.2 Pitting corrosion test

All other electrochemical tests were conducted with an electrochemical workstation PARSTAT2273, using the three electrodes cell. The samples were used as the working electrode, a saturated calomel electrode (SCE) was served as the reference electrode and a platinum foil was the counter one. The stable pitting behaviour was investigated through the critical pitting temperature (CPT) test in 3 mol/L NaCl aqueous solution, which is aggressive enough to accelerate the pitting process. By raising the temperature by 1 °C per minute at a constant potential of +700 mV (vs. SCE),

the value was defined as the temperature when the current increased irreversibly. All the CPT values obtained through this fast method were the average values after repeating for at least three times.

The pitting behaviour was also detected through the PPT in the same solution. The typical schematic diagram of PPT was showed in Fig.2, illustrating the square-wave potentiostatic pulse and its corresponding current-time curve. It could be found out that sometimes the current not recovered as the applied polarization potential dropping (marked with dot oval), which indicated that the pitting occurs randomly. For optimizing the parameters of this test, the Tafel polarization curves were measured in advance at the CPT of each sample separately, with a scan rate of 0.5 mV/s. Then the potential of CPT test +700 mV (vs. SCE) was chosen as the higher potential  $E_2$ , while one potential in the passive region of the Tafel curve was selected as the lower potential  $E_1$  for each sample. The duty cycle of  $t_1$  and  $t_2$  were set as 4 seconds and 2 seconds respectively to ensure the enough time for passivation after pulse, in other words, the pitting corrosion of the samples was under control.

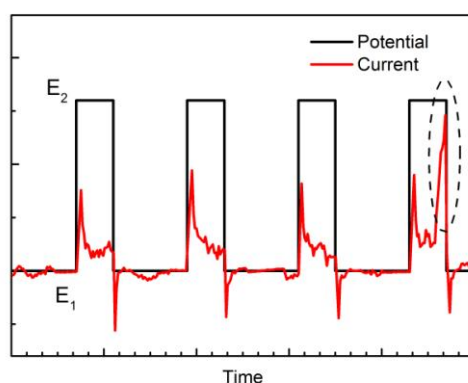


**Figure 2.** The potentiostatic pulse and corresponding current of PPT.

### 2.3. Morphology

The microstructure features were revealed by electrochemical etching in 10%wt ammonium persulphate solution, applying a constant current density of 1 A/cm<sup>2</sup> at room temperature. Here, ammonium persulphate solution was selected because it was more suitable for molybdenum-contained stainless steels [28] and sensitive to molybdenum-rich inclusions. The transmission electron microscope (TEM JEOL-2100F) with energy dispersive spectrometer (EDS) probe was used to identify the crystal structure and analysis the composition of precipitate phases.

## 3. RESULTS

### 3.1 The degradation of corrosion resistance after short-term aging

#### 3.1.1 Intergranular corrosion resistance

The weight loss rate of the specimens after boiling nitric acid immersion test was depicted in Fig.3, which was calculated according to the formula below:

$$\text{weight loss rate} = \frac{w_1 - w_2}{s \times t \times \rho}$$

w<sub>1</sub> — The weight of the specimens efore boiling nitric acid immersion test.

w<sub>2</sub> — The weight of the specimens after boiling nitric acid immersion test.

s — The total surface area of the specimens.

t — The duration of test.

ρ — The density of Type UNS31254 SASS.

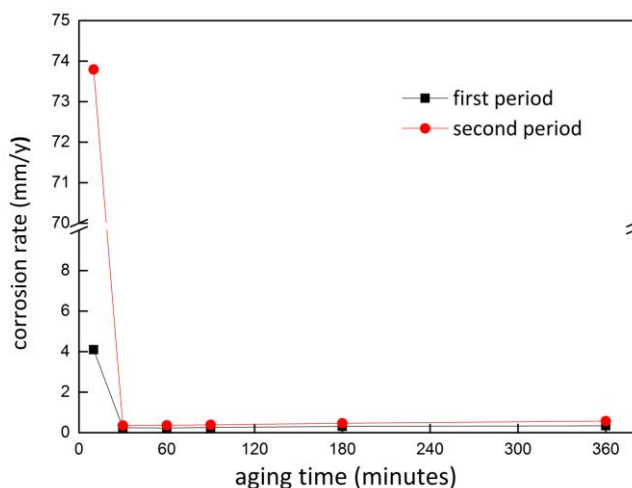


Figure 3. The weight loss rate of the specimens after boiling nitric acid immersion test.

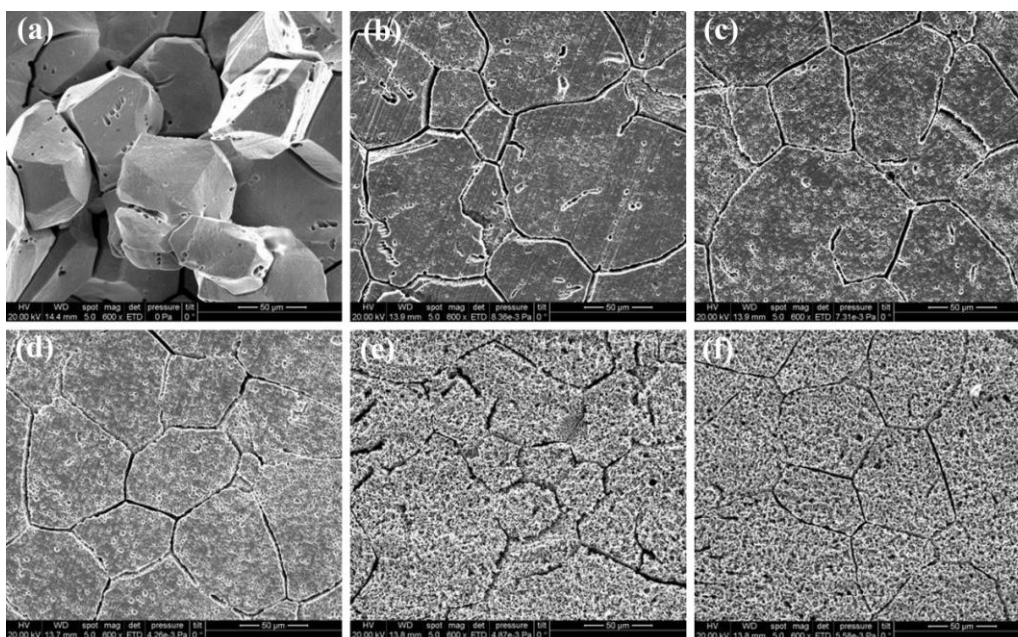


Figure 4. The morphology of the specimens after 2 periods boiling nitric acid immersion test:(a) 10mins; (b) 30mins; (c) 60mins; (d) 90mins; (e) 180mins; (f) 360mins.

Combining with morphology shown in Fig.4, although the grain size of the specimens was not changed evidently, serious intergranular corrosion was found after aging for only 10 minutes. Since the grain boundaries were terribly attacked, some grains even shed, which led to the high weight loss value of 73.79 mm/y. For 30 minutes, the weight loss rate dropped sharply to 0.35 mm/y. Then it remained at a relative low value with slight increase and was finally up to 0.57 mm/y at 360 minutes. In spite of the boundaries, the terrible corrosion was found inside the grains as well after 180 minutes, suggesting that the corrosion resistance tended to be uniform.

To UNS31254, which had a low level of carbon content and large amount of alloying element, the formation of intermetallic compound was the main factor that caused sensitization of intergranular corrosion. These phases preferentially formed along the grain boundaries, where the dislocation gathered and the energy barrier for precipitation was much lower [29]. Inasmuch as the boiling 65 wt% nitric acid applied a transpassive potential to the precipitations on samples immersed, they were dissolved and the ditches were left segmenting the grains. Therefore, through the prominently high weight loss rate and the morphology of the 10 minutes sample, it could be concluded that the precipitation formed along the boundaries even into networks and their dissolution made the some grains detach form the matrix. So this value could not represent the real intergranular resistance, but it could actually indicate the preferential sites of precipitations after such short term aging. As the aging going on, it provided enough time for alloying elements to full diffusion-migration and the composition discrepancy between the boundaries and interior eased. Hence the tendency of intergranular corrosion weakened and uniform corrosion occurred on the samples aging for 180 minutes.

### 3.1.2 The pitting corrosion resistance

The CPT values were listed in Table 2, which decreased gradually with the extension of the sensation time as expected. Moreover, it also demonstrated that the CPT dropped sharply from the first 180 minutes and then the degradation slowed down, which was in good accordance with the results of immersion tests. Meanwhile, the Tafel polarization curves were conducted at the CPT of the each specimen respectively, plotted in Fig.5. There were no active regions on all these curves and every test ended with the sudden incensement of the current, which indicated the formation and autocatalysis growth of stable pits. This critical potential was deemed as the pitting potential  $E_p$ .

**Table 2.** The average CPT values of UNS31254 after aging for different time (°C).

10min	30min	60min	90min	180min	360min
92	87	82.5	78	71	70

Based on the curves, the pitting potentials did not varied significantly as the CPT did, and all the values were concentrated at +600 mV (vs. SCE) around, except the sample of 360 minutes which

was approximately 150mV (vs. SCE) lower than the others. The fluctuation of the  $E_b$  was in the range of  $\pm 100$  mV (vs. SCE) after repeated experiments. Also, it could be observed that some metastable pits formed but soon recovered to be passive, which were manifested as the induced current on the passive region of polarization curves. Here, except obtaining some basic parameters of the pitting corrosion resistance, the experiments above mainly aimed to find out the optimum conditions for PPT measurements.

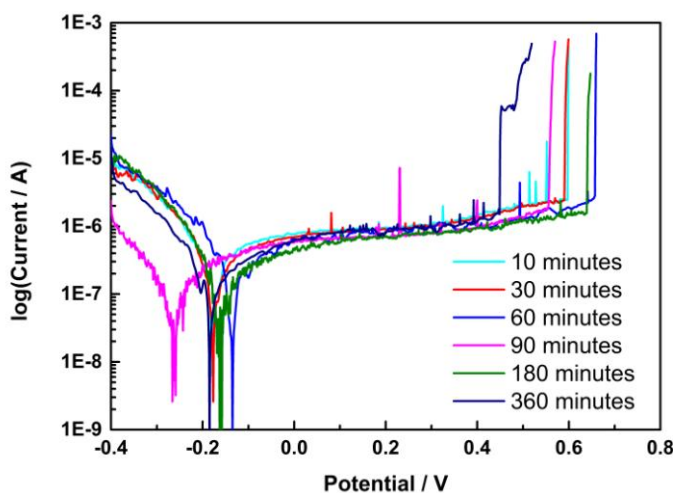


**Figure 5.** The polarization curves of the aging samples at CPT.

With the parameter above, the PPT was applied to detect the nucleating position of stable pits. The potential +700 mV (vs. SCE) was chosen as  $E_2$ , while lower one  $E_1$  was determined as +100 mV (vs. SCE), which was in the passive region for all the Tafel curves. All the experiments were conducted at the temperature slightly above their CPT. Thus the process of pitting corrosion was under control and 100 circles was applied for statistics. The morphology after etching for 1 minute was shown in Fig.6. From Fig.6 (a) - (d), stable pits which were larger than 20  $\mu\text{m}$  could be easily observed after test. However, in the Fig.6 (e) and (f), only uniform corrosion were found even after repeat experiments. Especially, Fig.6 (e) showed an intermediate state that flaws gathered near the border inside the grains while in Fig.6 (f) the grain were attacked uniformly after etching. These results were in complete agreement with immersion test, both of which buttressed the idea that type UNS31254 SASS was vulnerable to localized corrosion while aging within 180 minutes at 900  $^{\circ}\text{C}$ . Then as aging continued, the form of degradation transmitted into general corrosion, which was due to the ease of alloy-depleted zones and also presented as the deceleration of the CPT decline. Here, etching aimed to reveal the sites of stable pits. It could be discovered that the pitting preferentially occurred along the grain boundaries or at the triple joint, and some of them even involved the whole trivial grain. Taking the sample of 10 minutes for an example, the test curve was enclosed, shown in Fig.7. Despite those formed at the very beginning of the test, which showed high corresponding current, pits formed randomly for several times after the status of surface becoming steady. There were 15 stable pits found through SEM after test, and 14 of them were at the junction or on the grain boundaries. Combing with

the results of immersion tests, it was necessary to check the phases formed at the juncture of the grains, which seriously weakened the localized corrosion resistance of aged UNS31254.

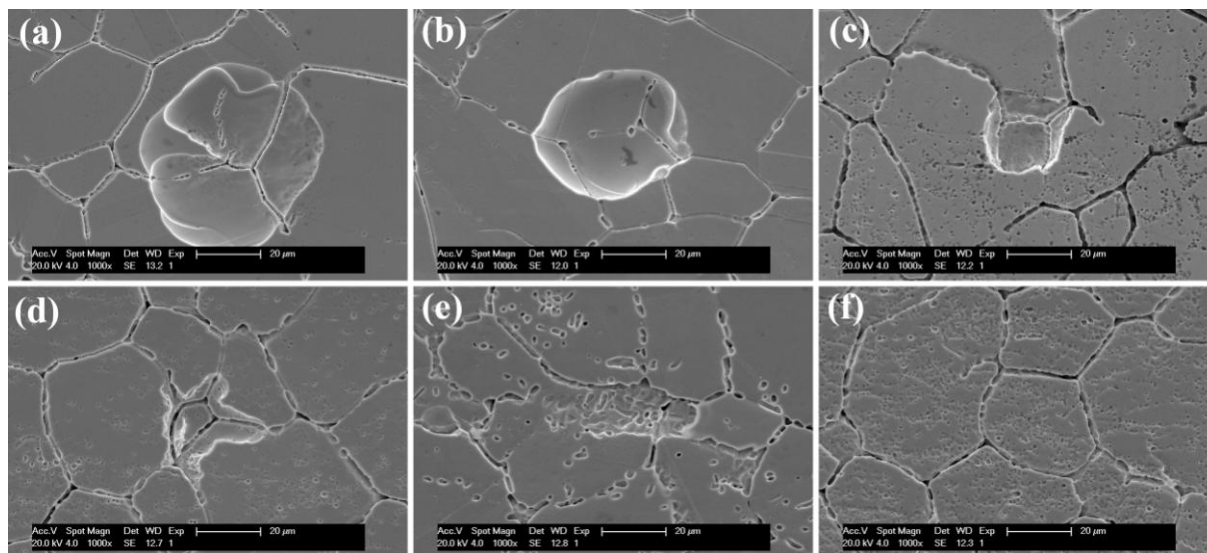


**Figure 6.** The morphology of the specimens after PPT tests:(a) 10min; (b) 30min; (c) 60min; (d) 90min; (e) 180min; (f) 360min.

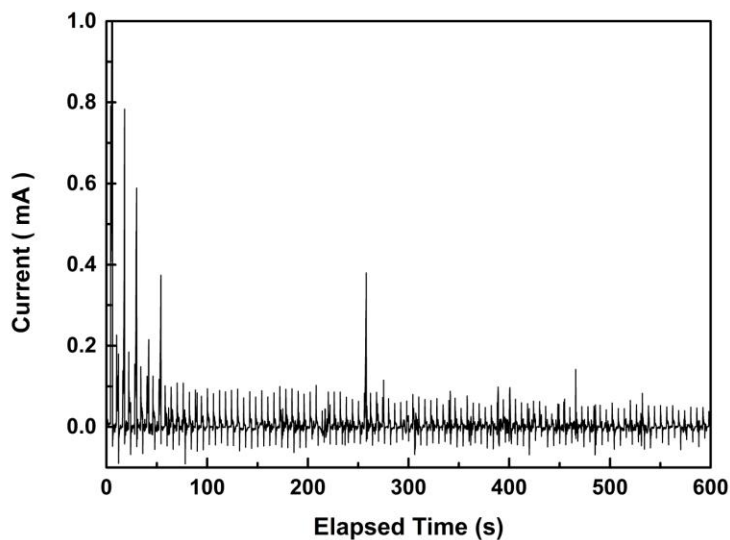
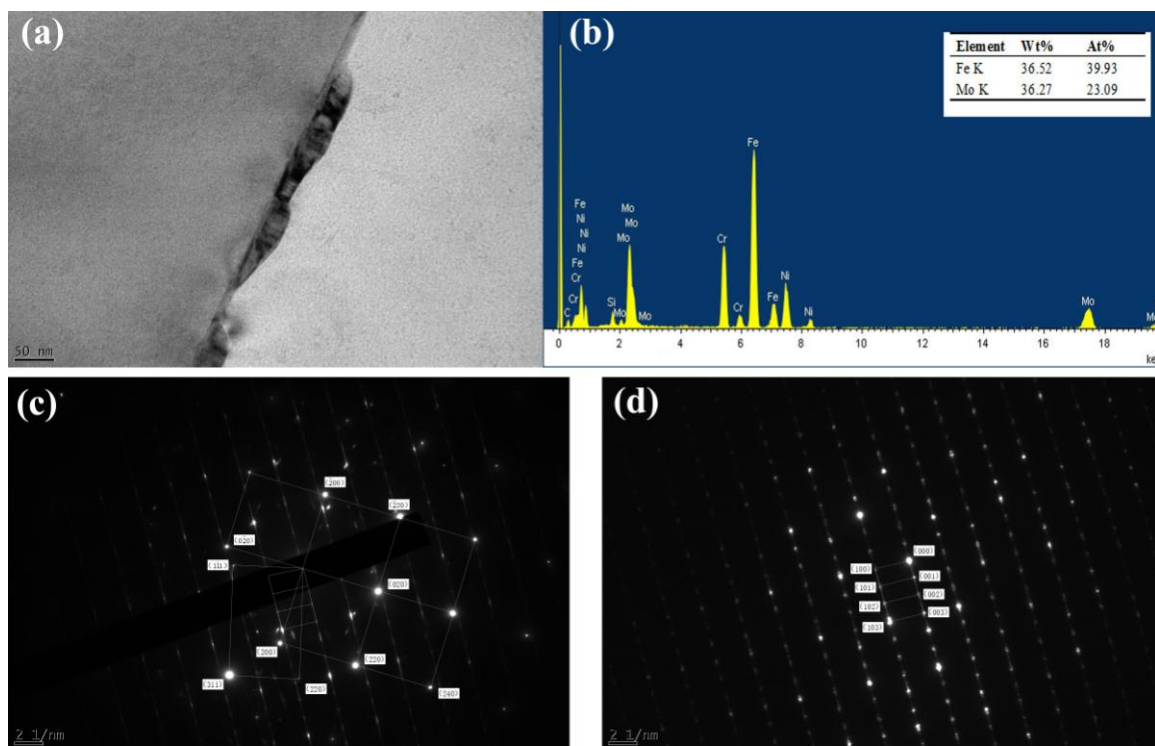


**Figure 7.** The PPT measurement curve of sample aging for 10 minutes.

### 3.2 Analysis of the intermetallic precipitates

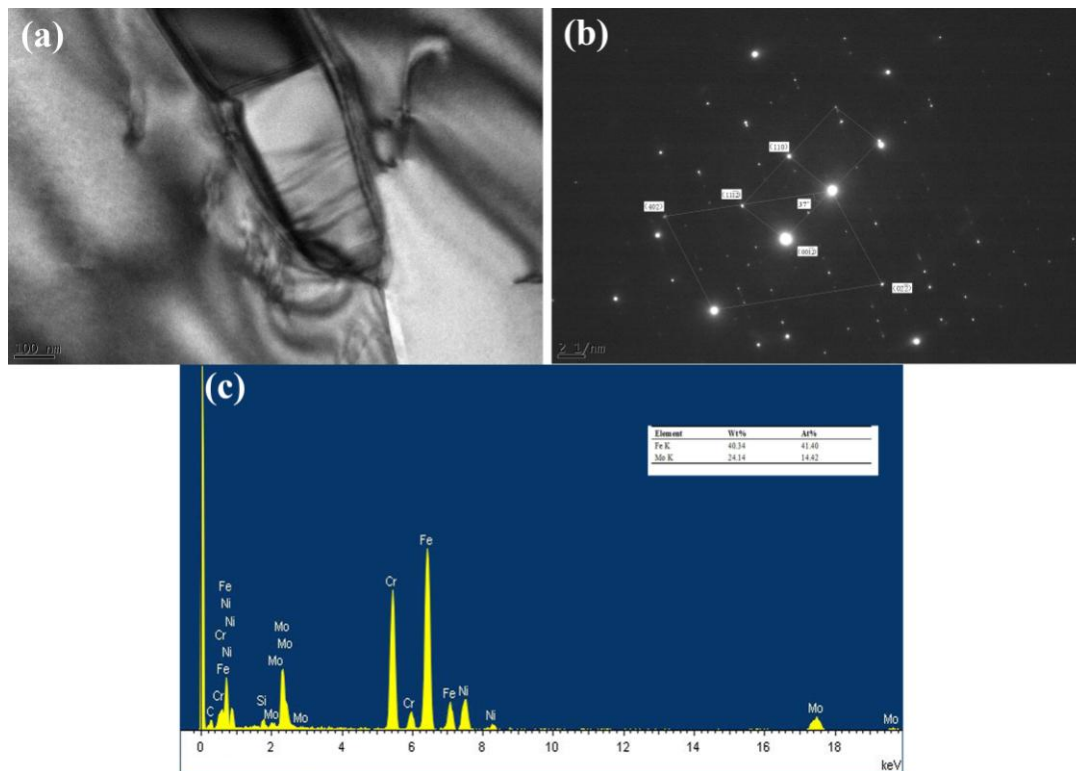
Examination via TEM was focus on the sample aged at 900 °C for 10 minutes, which also represented the influence of short-term heat treatment at the nose temperature on the time-temperature precipitation diagram. Fig.8 (a) showed the bright field images of the intermetallic phase and corresponding components. Morphologically, it maintained a relatively small size (less than 200nm in diameter) but seemed to form a continuous network along the grain through the bright field imagine.

Fig.8 (b) presented the composition of this phase. Comparing to the matrix, it was molybdenum-rich and accorded to the stoichiometry of  $AB_2$ . Its nano-beam electron diffraction (NBED) patterns in Fig.8 (c) further revealed it to be Laves phase. The crystal structure was confirmed to be a hexagonal cell unit, belonging to the space group  $P6_3/mmc$  with the lattice parameters  $a=4.73 \text{ \AA}$  and  $c=7.72 \text{ \AA}$ . Since it was heavily faulted, there were streaks and distortion in the obtained diffraction patterns along the  $\{0001\}$  direction. The orientation relationship was recorded in Fig.8 (d), which confirm the location of the precipitation and demonstrated that there was no definite angel relationship with matrix as well.



**Figure 8.** The identification of precipitation along the grain boundaries: (a) Bright field image; (b) Composition; (c) NBED patterns; (d) Electron diffraction patterns.

Another type of Laves phase were also found at the triple point junctions of the grains, which was shown in Fig.9 (a) – (d). It was identified as  $\mu$  phase through the electron pattern shown in Fig.9 (b). It belonged to the space group  $R\bar{3}m$  with the lattice parameters  $a=4.762 \text{ \AA}$  and  $c=25.61 \text{ \AA}$ , and it was a hexagonal cell unit as well. Its chemical formula was  $Fe_3Mo$  and contained nickel and chromium likewise. There has been reported that many binary Laves phases could dissolve the third element, like nickel and chromium, without varying their original crystallographic structure [30]. But that would bring some changes in the lattice parameters. For this reason, the deviation of lattice parameters and angle was in a reasonable range.



**Figure 9.** The precipitation at the triple joint:(a) Bright field image; (b) Electron diffraction patterns; (c) Composition.

Through the identification above, it could be concluded that the molybdenum-rich Laves-related phases caused the degradation of pitting and intergranular corrosion resistance. These phases concentrated molybdenum from the matrix, and made ambient deficiency of molybdenum, which is critical to passivation. Although the chromium plays an important part in forming the passive film, especially in acid solutions [31, 32], previous work also reported that the molybdenum also acted as a barrier preventing  $Fe^{3+}$  and  $Fe^{2+}$  to diffusing outside [33]. Coincidentally, in other types of high molybdenum stainless steels, it also helped to make the passive film more compact with different valence states [34]. All in all, such segregation led to the flaws of the passive film, which finally manifested as being vulnerable to intergranular corrosion and pitting on these sites. What’s more, Laves-related phases were usually deemed as metastable phases, which would transform into  $\sigma$  phase and perhaps  $\chi$  phase [18] if heating continued. Although the latter phases also concentrated lots of alloy element like chromium, their forming or transforming needed longer time, which made it possible for uniform diffusion of those element and the position of precipitation sites were not limited to the boundaries.

#### 4. DISCUSSION

Based on the conclusions drawn above, the pitting corrosion resistance of UNS31254 after welding process was investigated, during which the matrix could also be heated to a relative high

temperature and then cooled down rapidly. Generally, the temperature peak appeared near the weld pool in a range of 1200-1400 °C, which was named high temperature heat-affected zone (HTHAZ). It was expected that the prolonging of staying at high temperature led to an increase of the released precipitates amount, which finally decreased the resistance to pitting corrosion of HTHAZ. To qualify the degradation after welding, the welding heat curve shown in Fig.1 was simulated. It could be understood that both high heat-input and low cooling rate mean that the samples stayed at the sensitive temperature range for a long time. Through the variations of the average CPT values, described in Fig.10, the pitting corrosion resistance of UNS31254 decreased indeed as the heat-input increasing or the cooling rate descending. Since there was not enough time for precipitated phases to form in quantity and stably, the pitting corrosion resistance did not decline evidently comparing to the matrix.

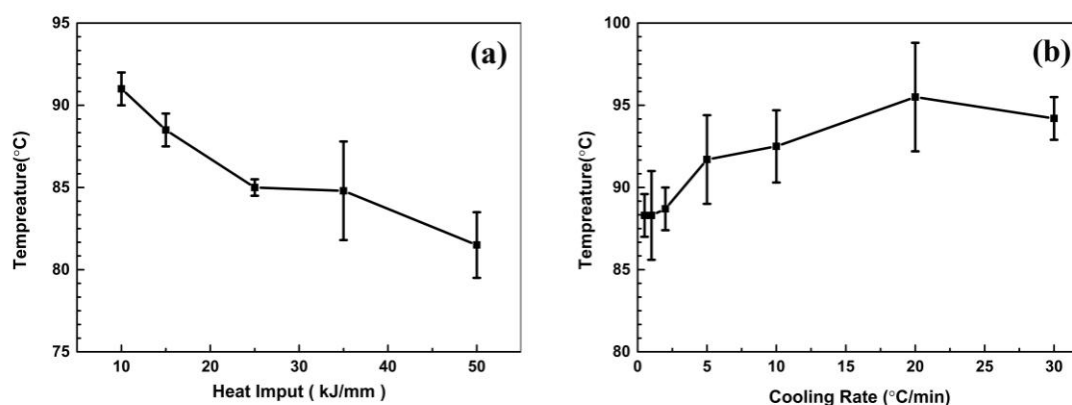


**Figure 10.** The CPT values of samples with different cooling rate and heat-input stimulating welding process.

Through the range of temperature values shown in Fig.10, it could also be discovered that the samples did not present perfect repeatability during the tests. Previous work had pointed out that the deviation was 6.6 °C when using static potential method to test CPT of UNS31254 matrix [35]. In addition, it had been reported that the CPT values of UNS31254 were independent of the  $\text{Cl}^-$  concentration in range of 1-5 mol/L NaCl [14-16]. This could be explained because once the occluded corrosion cell formed in the stable pits, the composition and concentration inside were much different from the bulk environment, which just offered the booster ions  $\text{Cl}^-$  to keep electric neutrality inside the pits. Here, although the 3 mol/L NaCl solution was chosen, according to the ASTM G150 [36] standard for electrochemical CPT test, the ceiling of this static potential method was to evaluate the SS which was equivalent to solution annealed UNS31254. That was to say the traditional test method could not meet the need for higher grade SASS and new approach should be attached to check their pitting corrosion resistance with different heat treatment history.

PPT could be the additional method because it further confirmed the critical condition of pitting corrosion, including CPT and pitting potential. In addition, it could be applied to detect precipitation sites statistically, and also find out the weak point on the surface. Moreover, as an

electrochemical test method, it could be conducted in lab and less time consuming. So this work recommend PPT as an attached method of SASS pitting corrosion test for pre-detection of precipitate phase and inclusions.

## 5. CONCLUSIONS

In this study of UNS31254, the corrosion resistance after short term heat treatment was investigated. Herein, the PPT was applied to detect the pitting corrosion sensitivity. After the identification of precipitate phases through TEM, the following results were obtained:

1. There was no change in grain size, but the corrosion resistance decreased evidently after short term aging at 900 °C. The ease of intergranular corrosion occurred after treating for 180 minutes, and the decrease of CPT values slowed down at the same time.

2. PPT test could be used to detect the nucleation sites of the precipitation sites. The morphology showed that the stable pits preferentially formed at the triple point junctions of grain boundaries, where the precipitation formed. Through the samples aging longer than 180 minutes, on which no stable pit was found, it could be further confirmed that the form of degradation transmitted from localized corrosion into general corrosion.

3. TEM results revealed that Laves related phase formed at 900 °C for only 10 minutes, which sample was heavily attacked through the immersion test. The  $\mu$  phase  $\text{Fe}_3\text{Mo}$  trended to nuclear at the triple point junctions whilst the Laves phase  $\text{Fe}_2\text{Mo}$  grew along the grain boundaries. The presence of Laves-related phases could break the integrity and the uniformity of passive film and leads the samples vulnerable to pitting and intergranular corrosion in chloride contained solutions.

## ACKNOWLEDGEMENT

The authors would like to acknowledge the helpful collaboration of Baosteel. This work is supported by the National Science Foundation of China (Grants No. 51371053, 51131008).

## Reference

1. C.J.O. Alonso, M.A. Lucio-Garcia, I.A. Hermoso-Diaz, J.G. Chacon-Nava, A. Martinez-Villafane and J.G. Gonzalez-Rodriguez, *Int. J. Electrochem. Sci.*, 9 (2014) 6717
2. X. Feng, X. Lu, L. Guo and D. Chen, *Int. J. Electrochem. Sci.*, 10 (2015) 10677
3. Y.A. Albrimi, A. Eddib, J. Douch, Y. Berghoute, M. Hamdani and R.M. Souto, *Int. J. Electrochem. Sci.*, 6 (2011) 4614
4. G. Gusmano, G. Montesperelli, G. Forte, E. Olzi and A. Benedetti, *Desalination*, 183 (2005) 187
5. J. Nordstrom and J. Olsson, *Desalination*, 97 (1994) 213
6. A. Al Odwani, M. Al-Tabtabaei and A. Abdel-Nabi, *Desalination*, 120 (1998) 73
7. A.K. Singh and G. Singh, *Anti-Corros. Method M.*, 49 (2002) 417
8. A. Malsnes and B. Hauge, *Zinc and Lead Processing*, (1998) 613
9. M. Oberndorfer, K. Thayer and M. Kastenbauer, *Mater. Corros.*, 55 (2004) 174
10. R. Singh and A.K. Singh, *Indian J. Chem. Technol.*, 9 (2002) 141
11. B. Wallen, M. Liljas and P. Stenvall, *Mater. Corros.*, 44 (1993) 83

12. C.J. Ortiz-Alonso, J.G. Gonzalez-Rodriguez, J. Uruchurtu-Chavarin and J.G. Chacon-Nava, *Int. J. Electrochem. Sci.*, 10 (2015) 5249
13. L. De Micheli, C.A. Barbosa, A.H.P. Andrade and S.M.L. Agostinho, *Br. Corros. J.*, 35 (2000) 297
14. R. Qvarfort, *Corros. Sci.*, 29 (1989) 987
15. E.A.A. El Meguid and A.A.A. El Latif, *Corros. Sci.*, 46 (2004) 2431
16. E.A.A. El Meguid and A.A.A. El Latif, *Corros. Sci.*, 49 (2007) 263
17. S. Ahmad and A.U. Malik, *J. Appl. Electrochem.*, 31 (2001) 1009
18. T. Koutsoukis, A. Redjaimia and G. Fourlaris, *Solid-Solid Phase Transformations in Inorganic Materials, Pts 1-2*, 172-174 (2011) 493
19. T. Koutsoukis, A. Redjaimia and G. Fourlaris, *Mater. Sci. Eng., A*, 561 (2013) 477
20. E. Pu, W. Zheng, J. Xiang, Z. Song, H. Feng and Y. Zhu, *Acta Metallurgica Sinica-English Letters*, 27 (2014) 313
21. S. Heino, *Metall. Mater. Trans. A*, 31 (2000) 1893
22. A. Von Keitz and G. Sauthoff, *Intermetallics*, 10 (2002) 497
23. J. Gao, Y. Jiang, B. Deng, Z. Ge and J. Li, *Electrochim. Acta*, 55 (2010) 4837
24. J.H. Kang and G.S. Frankel, *Z. Phys. Chem.*, 219 (2005) 1519
25. C.O.A. Olsson and D. Landolt, *Electrochim. Acta*, 48 (2003) 1093
26. S.M. Qidwai, V.G. DeGiorgi, A.C. Leung and Asme, *Proceedings of the Asme International Design Engineering Technical Conferences and Computers and Information in Engineering Conference, 2011, Vol 2, Pts a and B*, (2012) 161
27. ASTM A262, Standard Practices For Detecting Susceptibility To Intergranular Attack In Austenitic Stainless Steels, 2014
28. J. Reiter, C. Bernhard and H. Presslinger, *Mater. Charact.*, 59 (2008) 737
29. K.H. Lo, C.H. Shek and J.K.L. Lai, *Mater. Sci. Eng., R*, 65 (2009) 39
30. F. Stein, A. Palm and G. Sauthoff, *Intermetallics*, 13 (2005) 1056
31. I. Betova, M. Bojinov, T. Laitinen, K. Makela, P. Pohjanne and T. Saario, *Corros. Sci.*, 44 (2002) 2699
32. T.L.S.L. Wijesinghe and D.J. Blackwood, *J. Electrochem. Soc.*, 154 (2007) C16
33. C.T. Liu and J.K. Wu, *Corros. Sci.*, 49 (2007) 2198
34. R.M. Fernandez-Domene, E. Blasco-Tamarit, D.M. Garcia-Garcia and J. Garcia-Anton, *Thin Solid Films*, 558 (2014) 252
35. H. Andersen, C.O.A. Olsson and L. Wegrelius, *Electrochemical Methods in Corrosion Research Vi, Pts 1 and 2*, 289-2 (1998) 925
36. ASTM G150 - 13, Standard Test Method for Electrochemical Critical Pitting Temperature Testing of Stainless Steels, 2013